

Satellite-derived snow coverage related to hydropower production in Norway: present and future

J-G. WINTHER

Norwegian Polar Institute, 9296 Tromsø, Norway; e-mail: winter@npolar.no

D. K. HALL

NASA, Goddard Space Flight Center, Code 974, Greenbelt, MD 20771, USA

(Received 10 April 1998; in final form 28 January 1999)

Abstract. Hydropower derived from snow-melt runoff is a major source of electricity in Norway. Therefore, amount of snow-melt runoff is key to the prediction of available water. The prediction of water quantity may be accomplished through the use of hydrological models. These models, which may be run for individual basins, use satellite-derived snow-covered area in combination with snow-cover depletion curves. While it is known that snow albedo information would increase the accuracy of the models, large-scale albedo measurements have not yet been obtained from satellites on a regular basis. This paper presents Landsat-5 Thematic Mapper (TM) reflectances recorded in May 1989 from a mountainous catchment at Kvikne, Norway. Satellite-derived albedo values are analysed, and compared with simultaneously measured *in situ* albedo. The satellite-derived shortwave snow albedo is comparable with bare ground albedo and values as low as 0.19 were found in areas where the snow was highly metamorphosed and heavily blackened by organic material. To map snow-covered areas, the contrast between snow and snow-free areas can be improved by using a normalized TM Band 2–5 difference image. While TM Band 2 alone shows varying degrees of snow surface contamination within the study area, the normalized difference snow index (NDSI) is not affected by impurities. This paper also discusses the use of NASA's EOS (Earth Observing System) Moderate Resolution Imaging Spectroradiometer (MODIS) sensor, which is planned to be launched in the summer of 1999 for mapping of large-scale geophysical parameters including snow-cover. MODIS will enable snow cover and albedo to be mapped in Norway on a daily basis, and should enhance our ability to estimate snow coverage and thus manage hydropower production.

1. Introduction

Information from satellite sensors is commonly used in remote areas such as snow-covered mountainous terrain, especially when combined with point measurements of snow depth. Sensors with different spectral, temporal and spatial resolution are able to measure various snow properties, conditions and snow-covered areas. Next, snow in storage can be estimated from the percentage of terrain that is snow-covered. For example, Norwegian hydropower companies normally estimate the snow in storage by establishing a representative snow distribution curve that is

produced from many years of manual snow depth measurements along selected profiles (figure 1). When a representative snow-distribution curve for a certain catchment is established, the snow storage can be computed for any measured snow coverage, e.g. from satellite remote sensing. Subsequently, short- or long-term forecasts of watershed runoff for the spring flood season can be made (Andersen 1982, Martinec 1985).

The difference in reflective properties between snow and other surfaces is normally quite large, making it possible to distinguish and map snow-covered areas within a catchment. However, at the end of the snow-melt season the snow cover tends to become unevenly distributed, especially in mountainous areas. Numerous small patches of snow are surrounded by larger snow-free areas. Even within an image pixel, several surfaces with different characteristics might occur, creating mixed pixels. Under such conditions there are advantages gained by using satellites with high resolution to limit the number of mixed pixels. Additionally, the snow albedo at visible wavelengths is lowered due to contamination from surrounding snow-free areas while the on-going metamorphosis of the snow pack mostly affects the near-infrared (NIR) albedo.

Better knowledge of the variability of albedo, spectrally as well as in time and space, both for snow-covered and snow-free areas would be useful for a more accurate interpretation of satellite images, especially late in the melt season. Albedo is also useful as an input to hydrological models. In this study, field measurements of snow albedo, temperature, density and characterization of snow crystals together with meteorological and surface observations were collected simultaneously with a Landsat-5 Thematic Mapper (TM) overpass, from Kvikne, Norway, in May 1989. Normally, the snow disappears in late May/early June and accumulates in November in this area. Albedo recordings were carried out on a wide variety of surfaces to

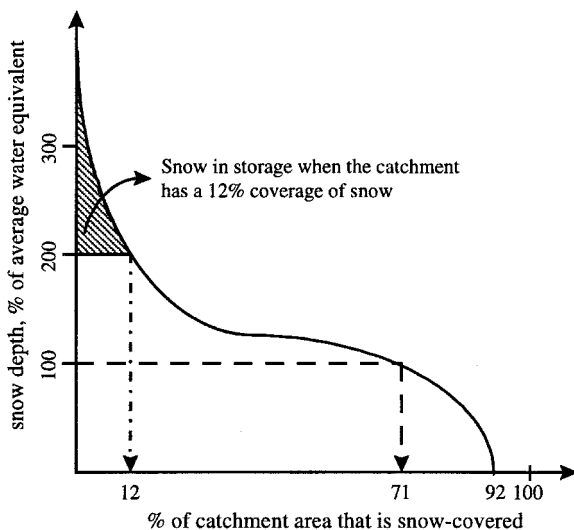


Figure 1. Schematic sketch showing the relationship between snow-covered area and snow in storage. Here, when the snow coverage reaches 12%, the snow in storage (m^3) is represented by the shaded area. A situation with on-going snow-melt can be illustrated by imagining the x -axis moving upwards and thus shrinking both the snow-covered area and the snow in storage.

study variability in reflectance, especially for snow. Later, supervised image training areas were selected to include the main surface categories, and subsequently analysed and compared with *in situ* snow albedo measurements. Furthermore, a normalized difference snow index (NDSI) was used to improve the contrast in the image.

Though Landsat TM has proven to be a useful tool for mapping of snow coverage, the sensor has limitations: data cannot be acquired through clouds, and it has only a 16-day repeat cycle. Thus, we welcome planned sensors, e.g. NASA's Landsat-7 Enhanced Thematic Mapper Plus (ETM+), Earth Observing System/Moderate Resolution Imaging Spectroradiometer (EOS/MODIS), and ESA's ENVISAT-1 Medium Resolution Imaging Spectrometer (MERIS), which are planned to be launched in spring 1999, summer 1999 and spring 2000, respectively. ETM+ will have eight channels in the visible to thermal-infrared (TIR) range with spatial resolutions of 30 m (visible and NIR) and 60 m (TIR). MERIS has 15 selectable bands across the range 0.4–1.05 μm with a spatial resolution of 300 or 1200 metres. Finally, MODIS will cover 36 bands in the range 0.4–14.4 μm with spatial resolution of 250 m to 1 km. In this paper, we describe the acquisition and utility of albedo measurements from the Landsat TM. We also discuss the utility of EOS/MODIS data for snow cover and albedo measurements, which will be useful for hydropower production management.

2. Hydropower production in Norway

In Norway, about 50% of the annual precipitation falls as snow. Furthermore, Norway produces nearly 100% of its electricity from hydropower. The total production capacity in a normal year is about 115 TWh. This puts special demands on models and other tools employed in managing this valuable water resource, and also on management for avoiding damaging situations such as flooding.

Today, snow-cover maps based on NOAA Advanced Very High Resolution Radiometer (AVHRR) data are used for management of hydropower production. The current algorithm for determining the snow cover from NOAA AVHRR is the Norwegian Linear Reflectance-to-Snow-Cover Algorithm (NLR) (Andersen 1982) which describes a linear relationship between areas of 0 and 100% snow coverage.

In order to generate hydroelectric power, snow-melt runoff is required. To predict snow-melt runoff, the snow-water equivalent (SWE) of the snow packs that contribute the meltwater must be determined. As mentioned, satellite data have proved very useful for monitoring snow-covered area and, with the use of depletion curves, for predicting SWE when input to hydrological models. The most commonly used hydrological model in Norway for this purpose is the precipitation-runoff model HBV. The HBV is a box model where input parameters are temperature and precipitation. These parameters are calculated for different elevation zones in a catchment based on standard temperature–elevation gradients, sometimes adjusted with data from automatic weather stations operated by local hydropower companies. Thus, the model keeps track of snow in storage for various elevation zones and simulates runoff from snow-melt.

In many regulated catchments in mountainous areas of Norway, a number of dams are located at different elevations and thus fed by areas on a sub-catchment scale. Proper management of these complex systems consisting of numerous dams, water pipes and connecting creeks/streams within sub-catchments spanning large elevation ranges demands updated information on snow in storage, especially in the snow-melt season. A corrected snow coverage derived from satellite data can be used to

update a HBV model and consequently improve the quality of runoff simulations needed for precise hydropower production management.

An additional input to other hydrological models is snow albedo which can be estimated from Landsat TM and other satellite data. Improved SWE and albedo inputs to hydrological models result in lowered errors in the prediction of snow-melt runoff.

3. Study area and *in situ* albedo measurements

Field measurements and image analyses were carried out within a 4.5 km × 4.5 km segment surrounding Lake Falningsjøen at Kvikne, Norway (figure 2). Elevations in the study area range from 843 to 1241 m a.s.l. Lake Falningsjøen is situated at 850 m a.s.l. While there is exposed rock in some areas, the terrain surface is mainly covered by moss, heather, bog, scrub and low birch wood.

Field measurements of albedo were collected consecutively at 12 different field stations using two simultaneously logging portable Aanderaa pyranometers, one up-looking and one down-looking (Winther 1989). The pyranometers have an effective wavelength range of 300–2500 nm. At each station 20 consecutive albedo measurements were recorded (figure 3).

Stations 1 to 6 were situated in totally snow-covered terrain with an albedo variation between 0.34 and 0.68. Stations 1 (slope 10° towards east) and 2 (horizontal) represent general snow conditions in the catchment. Stations 3 (horizontal), 4 (slope 5° towards the north-east) and 6 (slope 10° towards the north-east) are areas where the snow is heavily blackened by organic material such as moss, twigs, bark, lichen and leaves. At station 5 (horizontal), however, the snow was soaking wet and some puddles of water could be seen on the surface. The air temperature was well above zero during the 3-day field period and the snow was saturated and coarse grained. The variability in albedo values at each of the Stations 2, 4 and 5 is probably caused by slight movements in the stand where the pyranometers were fastened. Consequently, the surface area measured by the lower pyranometer could have varied during the series of consecutive measurements, causing an alteration in the recorded albedo. However, the large variations in albedo values *between* stations reflect the different surface characteristics. Temporal variability cannot be discerned from figure 3. Stations 7–12 (all horizontal) represent snow-free areas containing moss, heather and bog. The albedo ranged between 0.07 and 0.21 at these stations. All stations are located in the lower left quadrant of the indicated segment (figure 2).

4. Satellite sensor characteristics

4.1. *Thematic Mapper sensor characteristics*

TM Band 6 is in the thermal infrared part of the electromagnetic spectrum and has a spatial resolution of 120 m. TM Bands 1–5 and 7 are within the visible, near-infrared and medium-infrared wavelength regions and have spatial resolution of 28.5 m. Large variations in reflective characteristics caused by snow metamorphism and surface blackening occur at these wavelengths, making the bands suitable for studies of grain size and contamination (Dozier 1984). The analysed satellite image discussed in this paper is quadrant 3 of Landsat-5 TM, path 198 and row 16, recorded on 23 May 1989.

4.2. *Moderate Resolution Imaging Spectroradiometer (MODIS) characteristics*

MODIS is an imaging spectroradiometer that will provide imagery of the Earth's surface and clouds in 36 discrete spectral bands. The spectral bands cover parts of

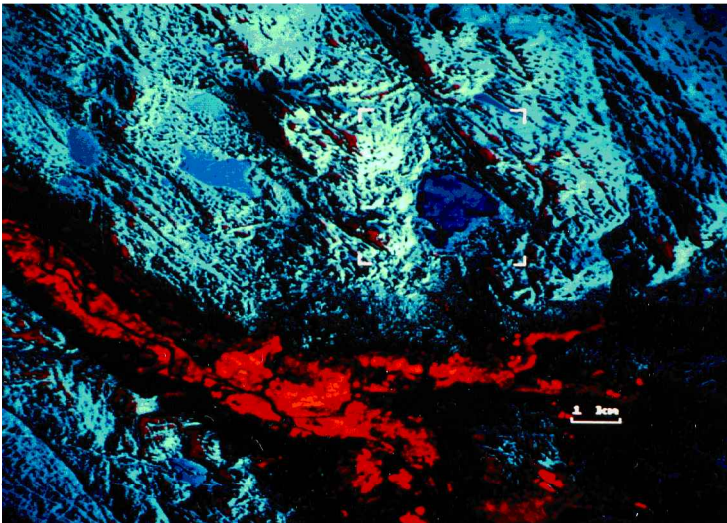


Figure 2. TM Bands 5, 4 and 2 colour composite recorded on 23 May 1989 showing the mountainous area of Kvikne, Norway. Field measurements and image analyses were performed within the indicated segment. North is towards the upper left and the solar elevation is 45.9° (from Winther 1992). Red colour represents agricultural land, dark green/black represents forested areas, blue/white represents snow, while brown (upper part of image) represents exposed rock at high elevations.

the electromagnetic spectrum from about 0.4 to 14.0 micrometres (table 1). The spatial resolution of the MODIS sensor at nadir will vary with spectral band and is 250m, 500m or 1 km. MODIS is scheduled for launch on the Earth Observation System (EOS) AM-1 polar-orbiting platform in the summer of 1999. Key land surface objectives are to study global vegetation and land cover, global land-surface change, vegetation properties, surface albedo, surface temperature and snow and ice cover on a daily or near-daily basis.

Mapping snow-cover extent and snow albedo using MODIS data will be advantageous because of the daily coverage in the high latitudes (cloud-cover permitting),

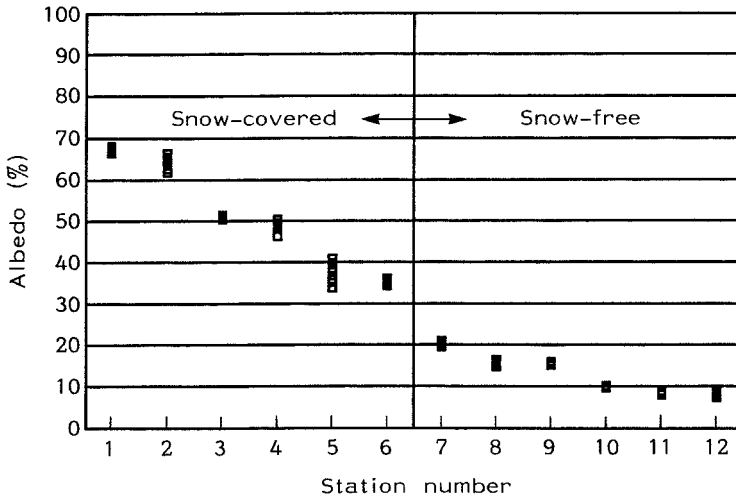


Figure 3. *In situ* measurements of shortwave albedo carried out on 22–24 May 1989 (from Winther 1992).

the improved spatial resolution, and the additional spectral bands, relative to current global-mapping sensors. MODIS bands 1–7 are likely to be useful for snow-cover and snow-albedo mapping (table 1). These represent discrete parts of the electromagnetic spectrum from 0.62 to 2.16 μm . Snow albedo may be calculated by interpolation between bands and using theoretical and measured reflectance curves for different snow types, and for mixed snow and vegetation.

While most of the first seven MODIS bands have a counterpart band on the Landsat TM and Enhanced Thematic Mapper Plus (ETM+) sensors, the TM and ETM+ sensors acquire data only every 16 days, cloud-cover permitting, and at a resolution that is excellent for catchment-scale studies, but not suitable for regional and global studies. The AVHRR sensors acquire data daily, but at 1.1-km resolution and currently without the use of the 1.6 μm band which is extremely useful for snow/cloud discrimination. As discussed later, there is a 1.6 μm band on the NOAA-15 AVHRR, which is currently operational, but the 1.6 μm band is not operational during the daytime, except for testing, and therefore is unavailable for use in regular snow-mapping studies. Future AVHRR sensors, however, will have the 1.6 μm band operating during the daytime hours.

MODIS will have the 1.6 μm band, 500-m spatial resolution in bands 1–7 and daily coverage of high latitudes, making it useful for snow-mapping studies, and complementary to the Landsat TM and ETM+ data for catchment-scale studies. MODIS will also have a daily cloud mask available as a MODIS product (Ackerman *et al.* 1998). This should further aid in snow mapping and snow/cloud discrimination.

At 500-m resolution, there will be mixed-pixel effects, as there will be no or few 'pure' pixels over land areas (with the exception of the ice sheets). Thus, the albedos will be influenced by both snow and vegetation cover. Additional problems concern high-cirrus clouds. Sometimes it is very difficult to detect high cirrus and the presence of these clouds will affect the measurement of albedo. Because of these and other limitations, the MODIS data will not be ideal but it is believed that MODIS will provide an enhancement over what is available today for snow-cover and -albedo mapping.

Table 1. MODIS technical specifications.

Primary use	Band	Bandwidth ¹	Spectral radiance ²	Required SNR ³
Land/cloud boundaries	1	620–670	21.8	128
Land/cloud properties	2	841–876	24.7	201
	3	459–479	35.3	243
	4	545–565	29.0	228
	5	1230–1250	5.4	74
	6	1628–1652	7.3	275
	7	2105–2155	1.0	110
Ocean colour/phytoplankton/biogeochemistry	8	405–420	44.9	880
	9	438–448	41.9	8380
	10	483–493	32.1	802
	11	526–536	27.9	754
	12	546–556	21.0	750
	13	662–672	9.5	910
	14	673–683	8.7	1087
	15	743–753	10.2	586
	16	862–877	6.2	516
Atmospheric water vapour	17	890–920	10.0	167
	18	931–941	3.6	57
	19	915–965	15.0	250
Primary use	Band	Bandwidth ¹	Spectral radiance ²	Required NE(Δ)T (K) ⁴
Surface/cloud temperature	20	3.660–3.840	0.45	0.05
	21	3.929–3.989	2.38	2.00
	22	3.929–3.989	0.67	0.07
	23	4.020–4.080	0.79	0.07
Atmospheric temperature	24	4.433–4.498	0.17	0.25
	25	4.482–4.549	0.59	0.25
Cirrus clouds	26	1.360–1.390	6.00	1504
	27	6.535–6.895	1.16	0.25
	28	7.175–7.475	2.18	0.25
	29	8.400–8.700	9.58	0.05
Ozone	30	9.580–9.880	3.69	0.25
Surface/cloud temperature	31	10.780–11.280	9.55	0.05
	32	11.770–12.270	8.94	0.05
Cloud top	33	13.185–13.485	4.52	0.25
	34	13.485–13.785	3.76	0.25
	35	13.785–14.085	3.11	0.25
	36	14.085–14.385	2.08	0.35

¹ Bands 1 to 19 are in nm; Bands 20 to 36 are in μm .² Spectral radiance values are ($\text{W m}^{-2} \mu\text{m}^{-1} \text{sr}^{-1}$).³ SNR = Signal-to-noise ratio.⁴ NE(Δ)T = Noise-equivalent temperature difference.

5. Landsat TM-derived surface albedo

Albedo is expressed as the ratio of total reflective radiation to total incident radiation. Total reflective radiation includes hemispherical surface reflection integrated over the reflective regions of the EM spectrum. Digital number (DN) given by the satellite image may be converted to surface albedo. The conversion is made in two steps. Firstly, spectral radiances in the image are calculated from the

DN (Markham and Barker 1986):

$$L_{\lambda} - LMIN_{\lambda} + \left[\frac{(LMAX_{\lambda} - LMIN_{\lambda})}{DNMAX} \right] DN \quad (1)$$

where L_{λ} is spectral radiance in the image ($\text{mW cm}^{-2} \text{ster}^{-1} \mu\text{m}^{-1}$); $DNMAX$ is maximum DN value for a particular band ($DNMAX = 255$ for all TM data); $LMIN_{\lambda}$ is spectral radiance at $DN = 0$; $LMAX_{\lambda}$ is spectral radiance at $DN = DNMAX$; $LMIN_{\lambda}$ and $LMAX_{\lambda}$ are given in Markham and Barker (1986).

Secondly, the effective at-satellite planetary reflectance is calculated from the spectral radiances:

$$\rho_p = \frac{\pi L_{\lambda} d^2}{ESUN_{\lambda} \cos \theta_s} \quad (2)$$

where d is Earth–Sun distance (AU); $ESUN_{\lambda}$ is mean solar exoatmospheric irradiance ($\text{mW cm}^{-2} \mu\text{m}^{-1}$); and θ_s is solar zenith angle (in degrees).

It should be noted that real planetary snow reflectances are higher than those calculated by equation (2) due to absorption and scattering in the atmosphere. Hall *et al.* (1990) applied atmospheric corrections to TM data acquired of Forbindels Glacier, Greenland, resulting in a 5–17% increase in reflectance relative to the at-satellite reflectance.

Additionally, equation (2) assumes effective reflectance from a surface which is 100% reflective and diffuse (Lambertian reflection). Freshly fallen snow can be considered nearly a Lambertian reflector, but the specular component tends to increase with the age of the snow cover, especially at low solar elevations (Steffen 1987). At the same solar elevation, forward reflection can be more prominent in the morning when the snow surface is glazed due to night-time refreezing of meltwater.

Eight training areas were selected within the study area shown in figure 2 using supervised classification with an ERDAS software system. The percentage covered by each training area within the study area is indicated in table 2. First, pixels were selected inside each of eight characteristic surface types chosen during the field measurement of albedo: density; wetness; air and snow temperature; slope and aspect; meteorological observations; surface contamination and roughness; time; and elevation (Winther 1989). Second, statistically similar areas were assigned to the original training areas using a maximum likelihood (Bayesian) classification method. Unclassified areas (6.4%) are mostly sun-exposed snow surfaces where detector

Table 2. Characteristics of the selected training areas.

Training area	Surface type	No. of pixels	% of total area
TR 1	Snow at the Lake Falningsjøen	5847	25.6
TR 2	Blackened snow: shore of lake Falningsjøen	1196	5.2
TR 3	Blackened snow on land	4859	21.3
TR 4	Clean snow, relatively flat terrain	3933	17.2
TR 5	Clean snow, sun-exposed terrain	1855	8.1
TR 6	Moss and heather	1305	5.7
TR 7	Mainly exposed rock	2319	10.2
TR 8	Open water	68	0.3
			SUM=93.6

saturation occurs, or areas where scrub and low birch stick out of the snow. Training areas were selected in horizontal terrain to minimize the effect of anisotropic snow reflection.

Analyses of spectral variations within and among training areas were performed using TM Bands 2, 4 and 5 (Winther 1992). These results are presented in table 3 and show at-satellite narrow-band albedo¹, atmospheric corrected narrow-band albedo², and atmospheric corrected shortwave albedo³, respectively. Evidently, large variations in brightness exist between the different training areas. The corrected narrow-band satellite albedo is converted to shortwave albedo (0.4–2.5 μm) to enable comparison with the *in situ* measurements by using methods reported by Nikol'skii (1973), Wiscombe and Warren (1980) and Hall *et al.* (1989).

Atmospherically corrected data are computed using the 5S computer code (Tanré *et al.* 1990). The 5S code allows estimation of solar radiation backscattered by the Earth surface–atmosphere system, as it is observed by a satellite sensor. For a specified ground reflectance the apparent or at-satellite reflectance is determined by the model. No clouds were present at Kvikne on the day of the Landsat TM overpass.

At-satellite reflectances were calculated for ground reflectances ranging from 0 to 1 with an increment of 0.1 for TM Bands 2, 4 and 5, and a look-up table was

Table 3. Reflective properties of the training areas using TM Bands 2, 4 and 5.

Training area	Band	Albedo ¹ and standard dev.	Albedo ² (atm. corr.)	Albedo ³ (0.4–2.5 μm)
TR 1 (snow on the lake)	TM2	0.45 ± 0.04	0.49	0.31
	TM4	0.33 ± 0.03	0.35	
	TM5	0.01 ± 0.00	0.01	
TR 2 (blackened snow)	TM2	0.33 ± 0.05	0.35	0.19
	TM4	0.21 ± 0.04	0.22	
	TM5	0.01 ± 0.00	0.01	
TR 3 (blackened snow)	TM2	0.52 ± 0.03	0.57	0.44 (0.50) [†]
	TM4	0.46 ± 0.03	0.50	
	TM5	0.01 ± 0.00	0.01	
TR 4 (clean snow)	TM2	0.61 ± 0.03	0.67	0.52 (0.64) [†]
	TM4	0.55 ± 0.02	0.59	
	TM5	0.01 ± 0.01	0.01	
TR 5 (clean snow)	TM2	0.73 ± 0.02	0.80	0.66
	TM4	0.69 ± 0.03	0.75	
	TM5	0.02 ± 0.01	0.02	
TR 6 (moss and heather)	TM2	0.18 ± 0.07	0.18	
	TM4	0.23 ± 0.03	0.26	
	TM5	0.14 ± 0.04	0.15	
TR 7 (exposed rock)	TM2	0.15 ± 0.01	0.15	
	TM4	0.23 ± 0.02	0.26	
	TM5	0.21 ± 0.01	0.23	
TR 8 (open water)	TM2	0.11 ± 0.02	0.10	
	TM4	0.05 ± 0.02	0.05	
	TM5	0.00 ± 0.00	0.00	

¹ Values are not corrected for gaseous absorption and molecule/aerosol scattering in the atmosphere.

² Atmospheric correction is executed (Tanré *et al.* 1990).

³ Narrow-band TM 4 albedos are converted into shortwave albedo (0.4 μm –3.0 μm) to enable comparison with field measurements (Hall *et al.* 1989).

⁴ Spectrally and geographically comparable field measurements (TR 3 and TR 4).

generated. Furthermore, simple linear regression using the at-satellite values as the independent variable (X) and ground reflectance as the dependent variable (Y) was carried out. Once regression equations were established, actual ground reflectance could easily be determined for every pixel. The error from using linear regression is negligible since the coefficient of determination, R^2 , is larger than 0.99 for all TM Bands (Winther 1992). The values in table 4 are *relative* and scaled to lie within the interval 0–1. Consequently, they are not directly comparable with the albedo values in table 3.

Scatterplots of TM5 and TM2, and TM5 and $(TM2 - TM5)/(TM2 + TM5)$, respectively, for the training areas (column 4 in table 3) are displayed in figure 4. The two scatterplots clearly demonstrate the improvement with respect to image

Table 4. Results and corresponding standard deviations from the normalized TM Band combinations.

	TR 1	TR 2	TR 3	TR 4	TR 5	TR 6	TR 7	TR 8
$TM \left(\frac{2-5}{2+5} \right)$	0.93 ± 0.02	0.90 ± 0.02	0.92 ± 0.03	0.92 ± 0.01	0.91 ± 0.05	0.17 ± 0.11	0.07 ± 0.02	0.91 ± 0.08

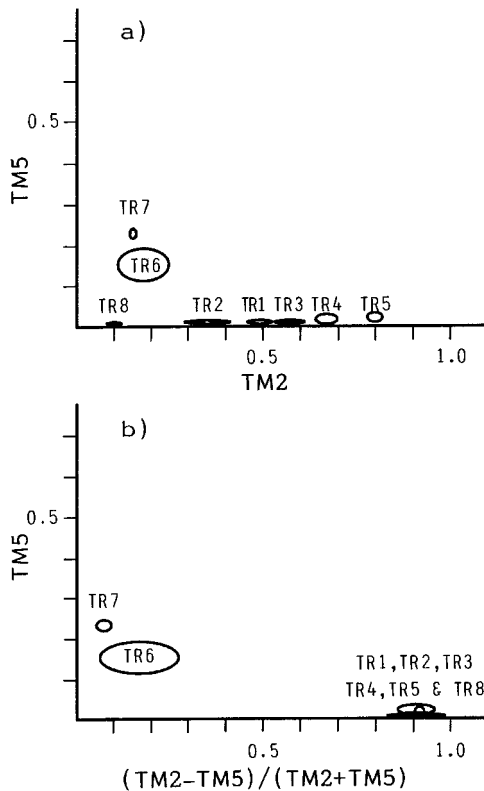


Figure 4. Scatterplots represent combinations of respectively (a) TM5 and TM2 and (b) TM5 and $(TM2 - TM5)/(TM2 + TM5)$. Ellipses indicate ± 1.0 . The separation between snow-covered areas and other surfaces is very good, the only exception being open water, which is included in the cluster of snow areas (from Winther 1992).

contrast using the normalized TM Band 2–5 difference image. In fact, this is not surprising, considering the spectral signatures of snow and soil (Lillesand and Kiefer 1987) (figure 5).

6. EOS Moderate Resolution Imaging Spectroradiometer (MODIS)

6.1. Description of the MODIS snow-mapping algorithms

Prototype snow-mapping algorithms have been developed to map snow using TM data as a surrogate for MODIS data. The algorithms are designed to detect snow, if present, in each pixel. Optimum detection of snow cover by reflectance properties requires that data be expressed in physical units, e.g. reflectance (see equation (2)). Then the normalized difference snow index (NDSI) is calculated.

In the original MODIS snow-mapping algorithm (Hall *et al.* 1995), snow is mapped in a pixel when the NDSI is greater than 0.4. In this binary classification, a pixel that is approximately 50% or more covered by snow is considered snow covered. Because the MODIS algorithm is an automated algorithm that is designed to map global snow cover, it was decided to produce a binary map, rather than a map that displays sub-pixel snow cover. Automated algorithms are not designed to map sub-pixel snow cover on the global scale, although work is progressing toward this end.

Water may also have an NDSI greater than 0.4, so an additional test is necessary to separate snow and water. Snow and water may be discriminated because the reflectance of water is $< 11\%$ in TM band 4; snow is mapped when the TM band 4 or the MAS channel 6 reflectance is $> 11\%$, and the NDSI is greater than 0.4. Frozen lakes are usually snow covered and therefore present no ambiguity. The large

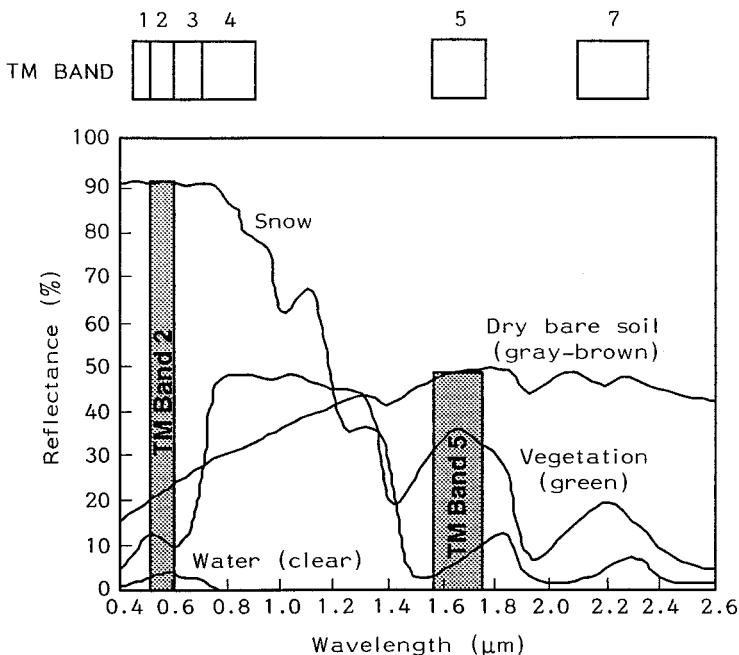


Figure 5. Typical spectral reflectance curves for snow, soil, vegetation and water (modified from Lillesand and Kiefer 1987, Wiscombe and Warren 1980).

lakes will be outlined on the snow maps by the land/water mask. Even if a lake is not snow covered, it will be mapped as snow, as long as it is ice covered.

In order to improve the algorithm so that it maps more snow in snow-covered forests, an enhancement of the original algorithm was developed (Klein *et al.* 1998). The major limitation in the original snow-mapping algorithm is that the 0.40 NDSI threshold is not well suited to the detection of snow in forests, as many snow-covered forests have an NDSI value below 0.40. However, these areas will have higher Normalized Difference Vegetation Index (NDVI) values. Thus, by using the NDSI and NDVI in combination it is possible to lower the NDSI threshold for forested pixels. The NDVI and NDSI are used together in order to discriminate between snow-free and snow-covered forests. The enhanced algorithm, employing both the NDSI and the NDVI, will be the at-launch MODIS snow-mapping algorithm.

6.2. Snow cover and albedo measurements using MODIS data

While the Landsat TM sensors are very useful for snow mapping on a given scene at a pixel resolution of 30 m, it is not feasible to monitor snow-melt using TM data because the Landsat satellite repeat cycle is 16 days. Advanced Very High Resolution Radiometer (AVHRR) data, however, are acquired daily at 1.1-km resolution, but AVHRR currently lacks the capability to discriminate snow and clouds, thus making snow mapping very difficult. While the NOAA-15 AVHRR has the 1.6 μm snow/cloud discrimination channel, data from that channel will not generally be available during daytime. Future NOAA satellites will fly sensors with the 1.6 μm channel operating during daylight hours. The MODIS will enable snow/cloud discrimination, and snow mapping at 500-m resolution (some snow mapping at 250-m resolution will also be possible). At the latitudes of Norway, MODIS will permit the daily monitoring of snow-melt in a catchment, cloud permitting. In addition, it will be possible to calculate snow albedo using MODIS data. Daily snow-cover products will be available from the National Snow and Ice Data Center (NSIDC) in Boulder, Colorado, at launch, and daily snow albedo maps will be available in the post-launch time frame.

In addition, combinations of optical and microwave data can provide even more accurate information which is of value for hydropower production. For example, while optical data distinguishes well between dry snow and bare ground and reasonably well between dry and wet snow, Synthetic Aperture Radar (SAR) separates wet snow from bare ground perhaps better than optical sensors do.

7. Factors that influence the albedo of snow

The albedo of snow depends on factors that can be categorized as follows: (i) physical, (ii) geometrical, and (iii) spectral characteristics. In the following sections we review the role of physical, geometrical and spectral characteristics as they affect the albedo, with special emphasis on factors relevant for this study.

7.1. Physical characteristics

The snow grain size, often expressed as the spherical grain radius, r , normally increases as the snow ages. The albedo is insensitive to grain size where the albedo is very high (in the visible) or very low (in the thermal infrared) but is highly sensitive in the near- and mid-infrared region, e.g. TM Band 4. The snow albedo drops at all wavelengths (VIS and NIR) as the grain size increases. Typically, grain size

growth at Kvikne during the snow-melt period occurs due to melt-freeze (MF) metamorphism, consequently building clusters of large grains.

Increasing liquid water content in the snow pack tends to lower the albedo. First, air is gradually replaced by liquid water between the ice grains when the snow pack starts to melt. Second, the spectral refractive index of liquid water is very close to that of ice for wavelengths smaller than $5\ \mu\text{m}$. Thus, the effect of liquid water is simply to increase the *effective* grain size which results in a decrease in snow albedo.

The spectrally integrated solar radiation flux diminishes rapidly on its way downwards through the snow pack due to both scattering and absorption. The absorption of solar radiation is greatest near the surface and is almost completely due to near-infrared absorption. The albedo of a thin snow pack depends on the albedo of the underlying surface. Wiscombe and Warren (1980) reported that the snow depth where one can start to 'see' the ground through the snow pack is approximately 20 cm. Solar radiation will penetrate deeper in a ripe snow pack than in a dry one (Gerland *et al.* in press). For remote sensing purposes it is of particular interest that (1) only the visible bands are sensitive to the effect of a thin snow pack and (2) the spectral albedo curve in the visible and near-infrared region flattens considerably when the snow pack thins. Field studies from Helligdagshaugen research site outside Trondheim, Norway, illustrate clearly the effect of snow depth on surface albedo (figure 6) (US Army Corps of Engineers 1956, O'Neill and Gray 1973, Winther 1993).

Model work by Choudhury and Chang (1979), Wiscombe and Warren (1980) and Warren (1982) conclude that snow albedo is independent of snow density. Thus,

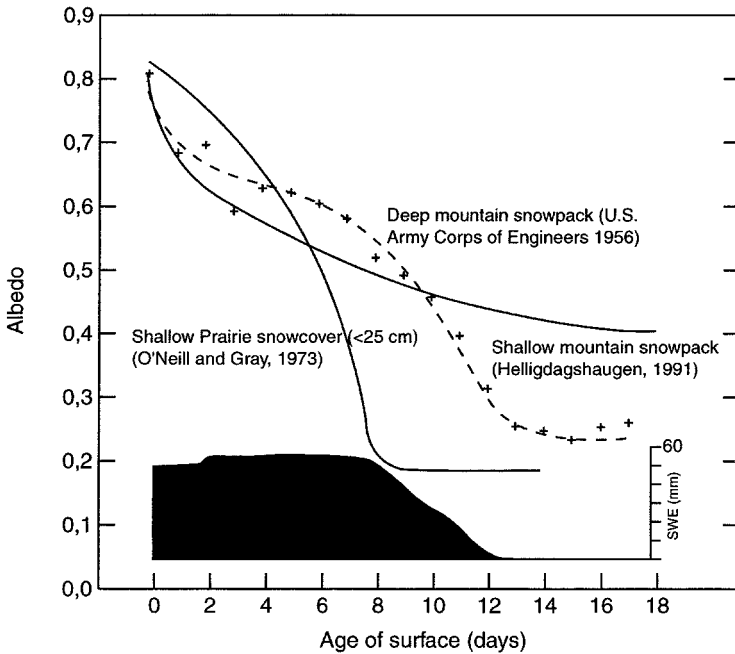


Figure 6. Temporal albedo variations of a melting snow pack and water equivalents at Helligdagshaugen compared with (1) a deep mountain snow pack (US Army Corps of Engineers 1956) and (2) a shallow Prairie snow cover (O'Neill and Gray 1973) (from Winther 1993).

the often observed dependence of albedo on density might actually be a dependence on grain size (Warren 1982). For the ripening snow pack at Kvikne, which undergoes MF metamorphism, the density increases with increasing grain sizes. Under other conditions, e.g. with a strong temperature gradient in the snow pack, depth-hoar formation predominates, and snow pack density will decrease with increasing grain sizes.

The thermal-infrared emission from snow is insensitive to snow pack parameters. For many purposes the snow emissivity is assumed to be equal to 1.0. The model used by Wiscombe and Warren (1980) calculates the snow emissivity using Kirchoff's radiation law:

$$e = 1 - a \quad (3)$$

where e is the emissivity and a is the albedo. When using data recorded by the near-nadir-viewing Landsat satellite where the thermal sensor (TM Band 6) is located between 10.40 and 12.50 μm , the snow emissivity can be assumed to be unity and considered independent of grain size. Even though TM Band 6 is not used in this study, thermal sensors can be used to distinguish melting snow (0°C) from dry (cold) snow, i.e. map areas of melting snow, which in turn is important for hydropower production management.

The impurities that have the most widespread effects on snow albedo are carbon soot, continental dust and volcanic ash (Warren 1984). The snow albedo is not affected by impurities beyond 0.9 μm . Finally, the snow albedo between 0.3 and 0.8 μm flattens out when dust is present in the snow pack (as for a thin snow pack). Knowledge about snow albedo variability is essential for accurate interpretation of satellite-derived snow coverage. For example, a blackened snow surface due to wind-blown transport of organic material from snow-free areas (which was the case at Kvikne) can be misinterpreted as bare ground during image classification.

7.2. Geometric characteristics

The albedo (a) is expressed as the ratio of reflected irradiance (E_r) to incident irradiance (E_i) (W m^{-2}):

$$a = E_r / E_i \quad (4)$$

Further, the bidirectional reflectance can be expressed as follows:

$$r(\theta_s, \theta, \phi) = R(\theta_s, \theta, \phi) / (E_i / \pi) \quad (5)$$

where $R(\theta_s, \theta, \phi)$ is the reflected radiance ($\text{W m}^{-2} \text{sr}^{-1}$). θ_s is the solar zenith angle for viewing angles θ and ϕ . The denominator is the diffuse radiance of a Lambertian reflector (i.e. 100% reflective) parallel to the surface. For an isotropic radiation field, R would be independent of the view angles, i.e. $a = r$. However, for anisotropic reflectance the deviation from isotropic reflection can be expressed by the anisotropic reflectance factor $f(\theta_s, \theta, \phi)$ as follows:

$$f(\theta_s, \theta, \phi) = R(\theta_s, \theta, \phi) / (E_r / \pi) \quad (6)$$

By combining equations (2), (3) and (4), the anisotropic reflectance factor can be expressed as the ratio of the bidirectional reflectance to the albedo:

$$f(\theta_s, \theta, \phi) = r(\theta_s, \theta, \phi) / a \quad (7)$$

A complete distribution of f as a function of $\theta \in [0, \pi/2]$ and $\phi \in [0, 2\pi]$ is called

the Bidirectional Reflectance Distribution Function (BRDF). To obtain accurate measurements of albedo from satellite-derived measurements of $r(\theta_s, \theta, \phi)$, the BRDF must be known (Knap and Reijmer 1998) (figure 7).

The effect of topography on surface albedo is partly implicit in the above formal description. More precisely, by introducing a topographic environment, the topography may (i) cast shadows on a pixel so that it receives no direct radiation at all, (ii) reduce the scattered sky radiation by hiding a part of the sky hemisphere, and (iii) reflect the radiation towards the pixel, consequently giving an additional irradiance. Obviously, the geometry between the sun, the target and the sensor might vary largely from one pixel to another. Therefore, field measurements and training areas were mostly chosen in horizontal terrain to minimize the effect of varying topography. The topographic effects are most pronounced at low solar elevations and for slopes close to the principal plane of the sun.

7.3. Spectral characteristics

The spectral characteristics of snow reflectance have been studied and reported by many investigators (Choudhury and Chang 1979, Wiscombe and Warren 1980, Warren 1982). The portion of radiation reflected from a surface consisting of fresh snow remains high in the visible region while a distinct drop occurs in the near-infrared region (figure 5). Furthermore, the snow albedo drops below 0.10 in the mid-infrared region where TM Band 5 (1.55–1.75 μm) and TM Band 7 (2.08–2.35 μm) are located. TM Bands 1, 2 and 3 are sensitive to visible blackening of the snow surface such as deposition of dust, volcanic ash and organic material (Dozier *et al.* 1981). Albedo reduction caused by snow grain coarsening is most prominent in the near-infrared region making TM Band 4 (0.76–0.90 μm) the most appropriate TM band for detection of snow metamorphosis processes.

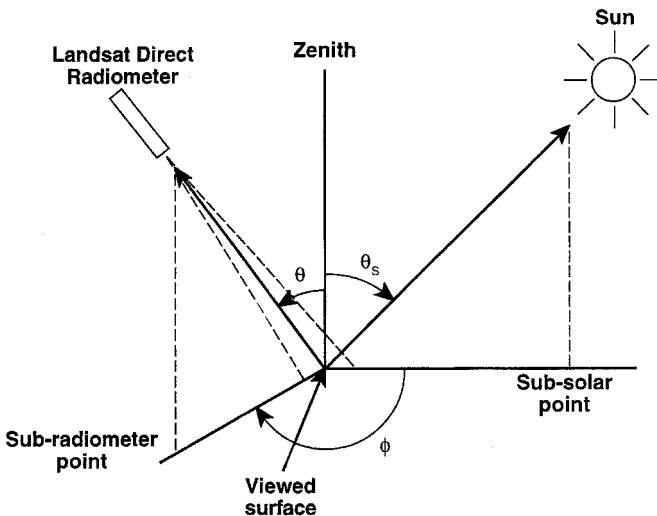


Figure 7. Sun-surface radiometer geometry. The view zenith angle, the relative view azimuth angle, and the solar zenith angle are denoted θ , ϕ , and θ_s , respectively (modified from Knap and Reijmer 1998).

TM Bands 2 and 5 may be used to distinguish snow from other surfaces. The normalized $(TM2 - TM5)/(TM2 + TM5)$ image generates high contrast between snow and snow-free areas (Kyle *et al.* 1978) and the normalized difference snow index (NDSI) is used as the basis of the MODIS snow-cover mapping algorithm (Hall *et al.* 1995, Klein *et al.* 1998). Spectral reflective curves show that this simple equation creates large positive values for areas covered by snow and smaller but negative values for dry, bare soil (figure 5).

7.4. Mixed pixels

The presence of a patchy snow pack is another factor affecting the retrieval of surface albedo from satellite data in mountainous regions, particularly in the melt season. Under such conditions, individual pixels can contain various surface types, often with widely differing reflective properties. Such was the case in the study area at Kvikne, which contained numerous patches of snow surrounded by snow-free areas, due to the advanced stage of melt at the time.

8. Conclusions

The spectral and spatial resolution of Landsat TM makes the sensor useful for detailed studies of reflective characteristics of snow and mapping of snow cover at the catchment scale. The shortwave snow albedo is highly variable in the snow-melt season; in this study it varies between 0.19 and 0.66. Surface contamination, high liquid water content in the snow pack combined with strong snow metamorphosis are reasons for the extremely low albedos found in the study area. Estimates of snow coverage, especially during melt conditions, are strongly improved by using the NDSI, and the normalized image is not affected by snow-surface contamination. Further, bidirectional reflectance increases as snow metamorphoses.

Landsat TM has demonstrated its ability for mapping snow covered areas, but the 16-day repeat period is a limitation for use in the snow-melt season when rapid changes take place and when normally there is a high percentage of days with cloud cover. Following the launch of the EOS/MODIS in the summer of 1999, daily, global snow cover will be acquired at a spatial resolution of 500m. The coarser-resolution MODIS data may complement and enhance the Landsat data, which will continue to be acquired from the Landsat-7 Enhanced Thematic Mapper Plus (ETM+), due to launch in the spring of 1999. In the post-launch time frame, a daily snow albedo product will also be available from MODIS. These products should improve our ability to map snow cover in catchments and to update hydrological models used in hydropower production management.

Acknowledgments

The authors would like to thank the following persons for their contributions: Ånund Killingveit and Knut Åmdal, Norwegian Institute of Technology, Turid Faanes, SINTEF Norwegian Hydrotechnical Laboratory, Clifford L. K. Robinson, Pacific Biological Station, and Jerry Maedel, University of British Columbia. Financial support has been provided from the Norwegian National Committee for Hydrology and the Fund for Licensing Fees (Konsesjonsavgiftsfondet).

References

- ACKERMAN, S. A., STRABALA, K. I., MENZEL, W. P., FREY, R. A., MOELLER, C. C., and GUMLEY, L. E., submitted, Discriminating clear sky from clouds with MODIS. *Journal of Geophysical Research*, **103**(D24), 32 141–32 157.
- ANDERSEN, T., 1982, Operational snow mapping by satellites. In *Hydrological Aspects of Alpine and High-Mountain Areas*, edited by J. W. Glen (IAHS Publication), pp. 138, 149–154.
- CHOUHDURY, B. J., and CHANG, A. T. C., 1979, Two-stream theory of reflectance of snow. *IEEE Transactions on Geoscience and Remote Sensing*, **17**, 63–68.
- DOZIER, J., 1984, Snow reflectance from LANDSAT-4 Thematic mapper. *IEEE Transactions on Geoscience and Remote Sensing*, **22**, 323–328.
- DOZIER, J., SCHNEIDER, S. R., and MCGINNIS, D. F., 1981, Effect of grain size and snowpack water equivalence on visible and near-infrared satellite observations of snow. *Water Resources Research*, **17**, 1213–1221.
- GERLAND, S., WINTHER, J.-G., ØRBAEK, J. B., LISTON, G. E., ØRITSLAND, N. A., BLANCO, A., and IVANOV, B., in press, Physical and optical properties of snow covering Arctic tundra on Svalbard. *Hydrological Processes*.
- HALL, D. K., BINDSCHADLER, R. A., FOSTER, J. L., CHANG, A. T. C., and SIDDALINGAIAH, H., 1990, Comparison of in situ and satellite-derived reflectances of Forbindels Glacier, Greenland. *International Journal of Remote Sensing*, **11**, 493–504.
- HALL, D. K., CHANG, A. T. C., FOSTER, J. L., BENSON, C. S., and KOVALICK, W. M., 1989, Comparison of in situ and Landsat derived reflectance of Alaskan glaciers. *Remote Sensing of Environment*, **28**, 23–31.
- HALL, D. K., RIGGS, G. A., and SALOMONSON, V. V., 1995, Development of methods for mapping global snow cover using Moderate Resolution Imaging Spectroradiometer data. *Remote Sensing of Environment*, **54**, 127–140.
- KLEIN, A. G., HALL, D. K., and RIGGS, G. A., 1998, Improving snow-cover mapping in forests through the use of a canopy reflectance model. *Hydrological Processes*, **12**, 1723–1744.
- KNAP, W. H., and REIJMER, C. H., 1998, Anisotropy of the reflected radiation field over melting glacier ice: Measurements in Landsat TM Bands 2 and 4. *Remote Sensing of Environment*, **65**, 93–104.
- KYLE, H. L., CURRAN, R. J., BARNES, W. L., and ESCOE, D., 1978, A cloud physics radiometer. *Third Conference on Atmospheric Radiation, American Meteorological Society, Davis, CA*, pp. 107–109.
- LILLESAND, T. M., and KIEFER, R., 1987, *Remote Sensing and Image Interpretation*, 2nd edn (New York: John Wiley & Sons).
- MARKHAM, B. L., and BARKER, J. L., 1986, Landsat MSS and TM post-calibration dynamic ranges, exoatmospheric reflectances and at-satellite temperatures. EOSAT technical notes, No. 1, 3–8.
- MARTINEC, J., 1985, Snowmelt runoff models for operational forecasts. *Nordic Hydrology*, **16**, 129–136.
- NIKOL'SKII, G. A., 1973, Integrated flux of direct solar radiation. In *Radiation Characteristics of the Atmosphere and the Earth's Surface*, edited by K. Ya Kondratyev (New Delhi: Amerind), pp. 289–328.
- O'NEILL, A. D. J., and GRAY, D. M., 1973, Spatial and temporal variations of the albedo of prairie snowpack. *The role of snow and ice in hydrology: Proceedings Banff Symposium, September 1972, Unesco-WHO-IAHS, Geneva-Budapest-Paris*, Vol. 1, pp. 176–186.
- STEFFEN, K., 1987, Bidirectional reflectances of snow. In *Large Scale Effects of Seasonal Snow Cover*, edited by B.E. Goodison, R.G. Barry and J. Dozier, *Proceedings of the IAHS Symposium, Vancouver, Canada*, pp. 415–425.
- TANRÉ, D., DEROO, C., DUHAUT, P., HERMAN, M., MORCRETTE, J. J., PERBOS, J., and DESCHAMPS, P. Y., 1990, Description of a computer code to simulate the satellite signal in the solar spectrum: the 55 code. *International Journal of Remote Sensing*, **11**, 659–668.
- U.S. ARMY CORPS OF ENGINEERS, 1956, Snow hydrology, summary report of snow investigations, Corps of Engineers, North Pacific Division, Portland, Oregon, pp. 141–191 and plates.
- WARREN, S. G., 1982, Optical properties of snow. *Reviews of Geophysics and Space Physics*, **20**, 67–89.

- WARREN, S. G., 1984, Impurities in snow: Effects on albedo and snowmelt. *Annals of Glaciology*, **5**, 177–179.
- WINTHER, J-G., 1989, Albedovariasjoner i snøsmeltesesongen (Albedo variations in the snow melt season). SINTEF report STF60 A89079. Norwegian Hydrotechnical Laboratory, Trondheim, Norway.
- WINTHER, J-G., 1992, Landsat Thematic Mapper (TM) derived reflectance from a mountainous watershed during the snow melt season. *Nordic Hydrology*, **23**, 273–290.
- WINTHER, J-G., 1993, Short- and long-term variability of snow albedo. *Nordic Hydrology*, **24**, 199–212.
- WISCOMBE, W. J., and WARREN, S. G., 1980, A model for the spectral albedo of snow. I: Pure snow. *Journal of the Atmospheric Sciences*, **37**, 2712–2733.